The Astrophysical Journal, 629:L117–L120, 2005 August 20

DISCOVERY OF A NEARLY EDGE-ON DISK AROUND HD 32297

Glenn Schneider,[1] Murray D. Silverstone,[1] and Dean C. Hines[2]

Received 2005 May 24; accepted 2005 July 14; published 2005 August 11

ABSTRACT

We report the discovery of a nearly edge-on disk about the A0 star HD 32297 seen in light scattered by the disk grains revealed in NICMOS PSF-subtracted coronagraphic images. The disk extends to a distance of at least 400 AU (3.″3) along its major axis with a 1.1 μm flux density of 4.81 $\pm$ 0.57 mJy beyond a radius of 0.″3 from the coronagraphically occulted star. The fraction of 1.1 μm starlight scattered by the disk, 0.0033 $\pm$ 0.0004, is comparable to its fractional excess emission at 25 + 60 μm of ~0.0027 as measured from *IRAS* data. The disk appears to be inclined 10.°5 $\pm$ 2.°5 from an edge-on viewing geometry, with its major axis oriented 236.°5 $\pm$ 1° eastward of north. The disk exhibits unequal brightness on opposing sides and a break in the surface brightness profile along the NE-side disk major axis. Such asymmetries might implicate the existence of one or more (unseen) planetary mass companions.

Subject headings: circumstellar matter — infrared: stars — planetary systems: protoplanetary disks — stars: individual (HD 32297)

1. INTRODUCTION

After decades of concerted effort applied to understanding the formation processes that gave birth to our solar system, until recently, the detailed morphology of circumstellar material that must eventually form planets has been virtually impossible to discern. The advent of high-contrast coronagraphic imaging, as implemented with the *Hubble Space Telescope* (*HST*) instruments, has dramatically enhanced our understanding of planetary system formation. Even so, only a handful of evolved disks ($\gtrsim 10^6$ yr) have been imaged and spatially resolved in light scattered from their constituent grains (e.g., Schneider et al. 1999; Weinberger et al. 1999; Ardila et al. 2004; Krist et al. 2005; Kalas et al. 2005). To expand this sample, we are conducting a Near-Infrared Camera and Multi-Object Spectrometer (NICMOS) coronagraphic imaging survey of 26 (typically $\gtrsim 10^7$ yr) main-sequence stars with strong thermal-IR excesses (indicative of circumstellar dust) to provide a larger ensemble of spatially resolved and photometrically reliable high-resolution images of debris disks, and to probe these posited epochs of planetary system formation and evolution. Our images shed light on the spatial distribution of the dust in disk systems, revealing disk structures as close as 0.″3 from their central stars. Here, we report our observations of HD 32297, which have given rise to the first new circumstellar disk image to emerge from our currently executing debris disk candidate survey.

2. OBSERVATIONS OF HD 32297

HD 32297 (A0; $d = 113 \pm 12$ pc [Perryman et al. 1997]; $J = 7.69$, $H = 7.62$, $K = 7.59$ [Cutri et al. 2003]) was highly ranked on our survey list because of its far-IR excess emission above the photospheric level, $f_{\rm ir} = L_{\rm disk,\,ir}/L_* \gtrsim 0.0027$, calculated from 25 and 60 μm fluxes in the *IRAS* Faint Source Catalog.

We conducted NICMOS observations of HD 32297 on 2005 February 24. Following F165M ($\lambda_{\rm eff} = 1.674$ μm, FWHM = 0.1985 μm) target acquisition (ACQ) imaging, deep coronagraphic (CORON) images were obtained in the F110W ($\lambda_{\rm eff} = 1.104$ μm, FWHM = 0.5915 μm) filter at two field orientation angles differing by 29.°2, yielding a total integration time of 1344 s (Table 1). Following the coronagraphic imaging at each field orientation, referenced by an *HST*/GO 10177 visit number (V*NN*) in this Letter, the spacecraft was slewed 2.″83, and the halo of the core-saturated unocculted (DIRECT) stellar point-spread function (PSF) was imaged.

3. CALIBRATION/REDUCTION

Basic calibration.—ACQ images were photometrically and astrometrically calibrated with procedures developed by the NICMOS Instrument Definition Team (IDT; Schneider 2002, hereafter SCH02, § 9). The raw MULTIACCUM (CORON and DIRECT) images were calibrated with the STSDAS CALNICA task (Bushouse 1997; Stobie et al. 1998). "Synthetic" dark frames, high S/N calibration reference flats, and linearity files appropriate for *HST* Cycle 13 were supplied by STScI. We augmented the STScI reference flat with data from contemporaneously acquired ACQ mode lamp flats in calibrating the CORON images (SCH02, § 8) because the imprint of the coronagraphic hole was shifted with respect to our images (Noll et al. 2004, § 5).

Reduction.—The three coronagraphic count rate images in each visit were median-combined, after verifying the stability of both the target pointing (SCH02, § 1) and the PSF (Schneider et al. 2001, hereafter SCH01, § 4) by examination of image pair differences. The two DIRECT images in each visit were similarly processed and then averaged. The combined calibrated images were post-processed to remove well-understood image/readout artifacts and those that arise in the presence of deeply exposed targets, e.g., (SCH02, § 8; SCH01, § 3; Schneider et al. 2003, § 3.1). The images were distortion-corrected by mapping input pixels with $X : Y$ scales of (75.950, 75.430) mas pixel^{-1} onto a rectilinear grid of 75.430 mas square pixels using the NICMOS IDT's IDP3 software (Schneider & Stobie 2002). Distortion-corrected instrumental count rates were converted to physical flux densities based on absolute photometric calibrations established from the *HST* SMOV3B program (F110W: 1.26 μJy (ADU s^{-1})$^{-1}$, $0_{\rm mag}$(Vega) = 1775 Jy; F165M: 3.00 μJy (ADU s^{-1})$^{-1}$, $0_{\rm mag}$(Vega) = 1022 Jy; M. Rieke 2002, private communication).

4. IMAGE REGISTRATION AND PSF SUBTRACTION

In each visit, the star's location in the CORON images was determined using spacecraft offset slew vectors downlinked in

[1] Steward Observatory, The University of Arizona, 933 North Cherry Avenue, Tucson, AZ 85721.
[2] Space Science Institute, 4750 Walnut Street, Suite 205 Boulder, CO 80301.

TABLE 1
NICMOS Observations of HD 32297

Visit	Orient[a]	Type	Filter	Readout Mode[b]	Exp. Time[c] (s)	Exp.	Data Sets
V43	201.57	ACQ	F165M	ACQ (ACCUM)	0.305	2	N8ZU43010
		CORON	F110W	STEP32/NSAMP14	224	3	…
		DIRECT	F110W	SCAMRR/NSAMP21	4.06	2	…
V44	230.77	ACQ	F165M	ACQ (ACCUM)	0.305	2	N8ZU44020
		CORON	F110W	STEP32/NSAMP14	224	3	…
		DIRECT	F110W	SCAMRR/NSAMP21	4.06	2	…

[a] Position angle of image *Y*-axis (east of north).
[b] See Noll et al. (2004).
[c] Expsoure time for each exposure (before combining).

the engineering telemetry applied to the star's position measured from the pre-slew ACQ image. Stellar image centroids were determined by Gaussian profile fitting, also using IDP3. The calibrated CORON images were co-aligned by shifting the V44 image to the location of the V43 image with IDP3's bicubic sinc function apodized interpolative resampling. With the images registered, simple image subtraction clearly showed the positive/rotated-negative signature of a nearly edge-on circumstellar disk.

Coronagraphic reference PSFs were aligned with the HD 32297 images in a similar manner. Our reference PSF images are generally drawn from the null detections in our survey that are all observed in very similarly constructed two-orientation orbits using nearly identical exposure sequences. These images were reduced, calibrated, and processed in the same manner as the HD 32297 images. To qualify as a reference PSF, the star must be at least as bright as the disk target star, and of similar spectral type to minimize color effects under the F110W filter. Additionally, we applied a coronagraphic PSF from HD 9627, a very bright calibration target of nearly identical spectral type that was previously observed coronagraphically and found not to possess any detectable disk-scattered light. On 2004 December 22 the *HST* secondary mirror was moved,[3] causing small, but noticeable, differences in the coronagraphic PSF structure in subsequent images. Hence, reference PSF stars for HD 32297 were restricted to stars observed after that date. For our HD 32297 PSF subtractions, four of our stars met the above criteria: HD 9627 (A1 V, $J = 5.49$; V84), HD 142666 (A8 V, $J = 7.35$; V2B and V2C), HD 36112 (A3, $J = 7.22$; V31 and V32), and HD 83870 (F8, $J = 6.73$; V61 and V62); the J magnitudes are from Cutri et al. (2003).

We separately registered and subtracted all seven PSF star images after scaling their intensities, separately, from both the V43 and V44 images of HD 32297 (see SCH01 for details of process and error estimation). We used our DIRECT images of the stars to estimate the flux density scaling for the reference PSFs. After co-aligning the DIRECT images, we performed iterative subtractions to null the star images (masking saturated pixels) and establish the intensity ratios. After subtracting each PSF from the V43 and V44 target observations, the ensemble of PSF-subtracted disk images exhibited some degree of variation. The subtractions using HD 142666 and HD 36112, which are anomalously red for A stars, produced zonal under- and oversubtractions at different radii, indicative of target : reference PSF differences from mismatched spectral energy distributions.

[3] See http://www.stsci.edu/hst/observatory/focus/mirrormoves.html.

5. DISK IMAGES

Serendipitously, the near–edge-on disk is favorably oriented with respect to the *HST* diffraction spikes and is revealed with very similar morphology in all 14 PSF subtractions. Importantly, all PSF-subtracted images from both HD 32297 visits show the same disk structures at both field orientations. The fine structures in the V61 HD 83870 PSF halo and diffraction spikes were most closely matched to those in the V43 image of HD 32297. This subtraction, shown in Figure 1, produced the most artifact-free image after alignment ([+0.304, +0.143] pixel shift) and intensity scaling by 0.440 ± 0.005. The measures we discuss in § 6 were made from this image. We assess the systematic errors in these measures using an ensemble of six PSF-subtracted images from (V43, V44) and (V61, V62, and V84), all measured identically. As a test, we subtracted the three selected reference PSFs from each other, and no evidence of any disklike "features" was found. We disqualified the HD 142666 and HD 36112 PSF subtractions from the quantitative error estimation for the reasons noted in § 4.

6. RESULTS

Disk geometry.—The HD 32297 disk extends ≳3.″3 (400 AU) to the northeast (NE) of the star and ≳2.″5 toward the southwest (SW; 3 σ lower limits; see Fig. 2; the depth of our integrations limits our sensitivity to low surface brightness flux in the outer regions of the disk). Assuming intrinsic circular symmetry, by isophotal ellipse fitting we find the disk inclined 10.°5 ± 2.°5 from an edge-on viewing geometry with a major-axis position angle P.A. = 236.°5 ± 1°.

Disk brightness.—We measured the total (area-integrated) disk brightness, excluding the $r < 0.''3$ coronagraphically obscured region, as 4.81 ± 0.57 mJy. We used a 7.″049 (93 pixel) × 0.″682 (9 pixel) rectangular photometric aperture centered on the star with its long axis parallel to the disk major axis. The aperture was sufficiently long and wide to capture all the measurable disk flux, as was tested by incrementally increasing the aperture size. Bifurcating the aperture, we find no statistically significant difference in the total disk flux above (56% ± 12%) and below (44% ± 12%) the disk midplane.

Scattering fraction.—Because our DIRECT images are core-saturated, we used HD 32297's spectral type and Two Micron All Sky Survey (2MASS) catalog magnitudes to establish the brightness of the star in the F110W passband.

We used the STSDAS CALCPHOT task to transform 2MASS magnitudes to the NICMOS filter system and found F110W = 7.71 ± 0.03 mag, with a corresponding 1.1 μm stellar flux density of 1.46 ± 0.04 Jy. We tested the robustness of this procedure by transforming the 2MASS photometry to

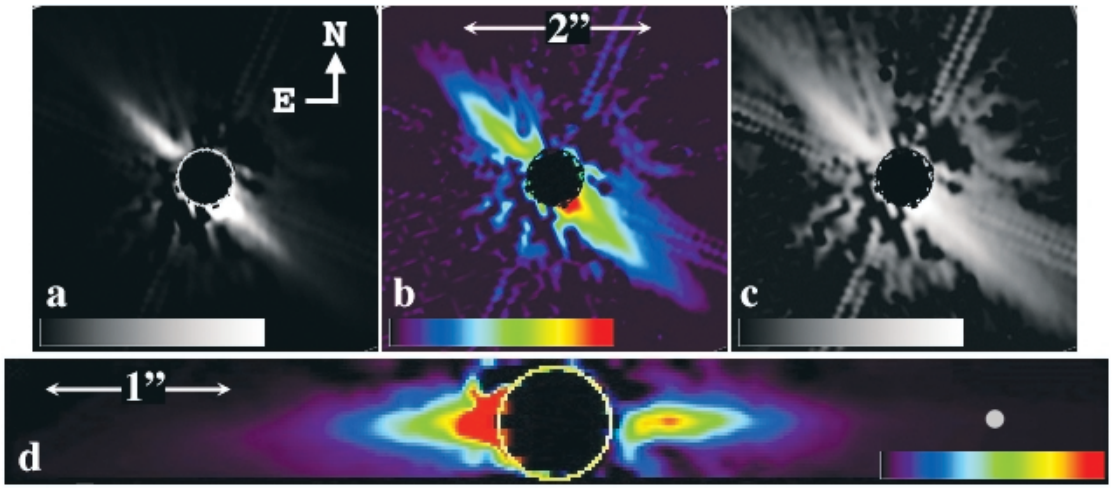

FIG. 1.—V43–V61 PSF-subtracted image of the HD 32297 circumstellar disk. The central circle in each panel indicates the $r = 0\farcs3$ coronagraphic hole. (*a*) Linear display: 0–11 mJy arcsec^{-2}. (*b*) The $\log_{10}$ display: [−0.7] to [+1.7] mJy arcsec^{-2}. (*c*) The $\log_{10}$ display: [−1.5] to [+1.5] mJy arcsec^{-2}. (*d*) Horizontally oriented major axis. The small gray circle indicates the size of a 0.″11 resolution element. Linear display: 0–12 mJy arcsec^{-2}.

the NICMOS F165M band. The F165M magnitude of HD 32297 measured from our ACQ images is 7.61 ± 0.03, in agreement with the CALCPHOT prediction of 7.61 ± 0.05. We then find that the fraction of 1.1 μm starlight scattered by the disk, $f_{\rm nir} = L_{\rm disk,\,nir}/L_{*,\,\rm nir}$, for $r > 0\farcs3$, is 0.0033 ± 0.0004.

Radial surface brightness profile.—We measured the surface brightness (SB) of the disk along its major axis in both directions from the star in square apertures one resolution element (very close to 1.5 pixels) in extent and spaced one resolution element apart to provide independent measures in every other sample. The measured flux densities were converted to SB units, and the major-axis radial profiles of both "halves" of the disk are shown in Figure 2. Our photometric measurement uncertainties, on spatial scales of a resolution element, are dominated by residuals from imperfect PSF subtractions. Because of the disk's ~10° inclination, there is no significant disk flux along, and near, the minor axis beyond the radius of the coronagraphic hole. Hence, we measure 1 σ background variations along three radials (six points at each radius) roughly orthogonal to the disk centered on the minor axis (but avoiding the diffraction spike) to estimate the measurement uncertainties arising from subtraction residuals at equal radial distances along the major axis. These measures are made identically to the disk flux measures along the major axis. Beyond ~ 2.″2, where the read noise becomes significant, the uncertainties (Fig. 2 error bars) grow larger as a fraction of the disk flux.

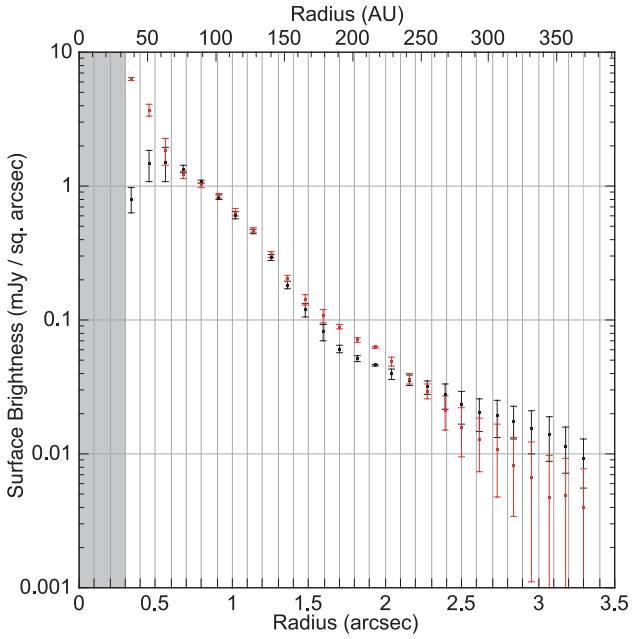

FIG. 2.—Radial SB profiles along NE (*black*) and SW (*red*) "halves" of the HD 32297 disk major axis. The 1 σ error bars estimate uncertainties from background variations and do not include the ~12% uncertainty in the absolute calibration of the disk flux. The first resolution element beyond the obscured (*gray*) region may be affected by coronagraphic hole edge effects.

Disk asymmetries.—The SW side of the disk (at $r > 0\farcs3$) is brighter (3.14 ± 0.57 mJy) than the NE side (1.67 ± 0.57 mJy). In all HD 32297 PSF-subtracted images, at both field orientations, the SW side of the disk is brighter near the star (e.g., at $r < 0\farcs6$ in the V43–V61 major-axis radial profile; Fig. 2). The innermost point in the radial profiles (at 0.″35) on opposite sides of the disk is questionable due to its close proximity to the edge of the coronagraphic hole, and it should be viewed with caution. This brightness asymmetry, however, extends several hundred milliarcseconds farther out and is also seen above and below the midplane of the disk (e.g., Fig. 1*d*).

The SW and NE profiles are symmetric from $0\farcs5 < r < 1\farcs7$, while they differ significantly at smaller and larger radii. The SB profile (SB in units of mJy arcsec^{-2}, r in arcseconds) of the SW side of the disk at $r > 0\farcs5$ is well represented by a power law: SB(SW) $= 0.455r^{-3.57}$ with a goodness of fit $R^2 = 0.996$. Fitting a single power law to the NE side of the disk, SB(NE) $= 0.45r^{-3.2}$ ($R^2 = 0.931$), does not do as well. By inspection, there is an obvious "break" in the NE SB profile (Fig. 2) at $r = 1\farcs7$. In this region ($1\farcs4 < r < 2\farcs1$), the NE side SB is systematically lower than the SW side SB. Separately fitting the regions on both sides of the break yields SB(NE; $0\farcs5 < r < 1\farcs7$) $= 0.51r^{-3.7}$ ($R^2 = 0.940$) and SB(NE; $1\farcs7 < r < 3\farcs4$) $= 0.286r^{-2.74}$ ($R^2 = 0.996$).

7. DISCUSSION

HD 32297 joins β Pic, HR 4796A, and α Psc A as an additional example of a scattered-light disk about an A-type

TABLE 2
DUSTY DISKS AROUND A STARS

Parameter	HD 32297	β Pictoris[a]	HR 4796A[b]	HD 141569A[c]	Fomalhaut[d]
Spectral type	A0	A5	A0	Herbig Ae/Be (B9.5)	A3
Est. age (Myr)	??	12–20	8	5	200
Disk radius (AU)	400	~1600[e]	70	400	141
$f_{\rm nir}$	0.0033	~0.003[f]	0.0024	0.0025	10^{-6}
$f_{\rm ir}$	0.0027	0.0015[g]	0.005	0.0084	5×10^{-5}[g]
Anisotropies	See § 6	…[a]	…[b]	…[h]	…[d]

REFERENCES.—(a) Kalas & Jewitt 1995; (b) Schneider et al. 1999; (c) Weinberger et al. 1999; (d) Kalas et al. 2005; (e) Larwood & Kalas 2001; (f) Estimated from Kalas et al. 2000; (g) Decin et al. 2003; (h) Clampin et al. 2003.

star. One might consider in comparison the optically thin disk of the Herbig Ae/Be (B9.5) star HD 141569A, although this may represent an example of a transitional disk about a star younger than either β Pic or HR 4796A. Table 2 summarizes the characteristics of all five disk systems.

HD 32297 is located at the bottom of the A star main-sequence locus in a M_V versus $B - V$ color-magnitude diagram (see Jura et al. 1998). Its low luminosity ($M_V = +2.88$ [+0.27, −0.24]; Perryman et al. 1997) is similar, for its $B - V$ color ($+0.199 \pm 0.014$), to β Pic and HR 4796A, suggestive of youth comparable to these stars with ages of $\sim 10^7$ yr (Jura et al. 1998). While HD 32297's age is not well constrained, both its $f_{\rm nir}$ and $f_{\rm ir}$ are also comparable to these young stars' and to HD 141569A's, but hundreds of times larger than the much older α Psc A's.

The HD 32297 disk is intermediate in size between the very large β Pic disk and the width/radius ≈ 0.2 debris rings circumscribing HR 4769A and α Psc A, but is comparable in size to the HD 141569A disk. Dust in the β Pic and HR 4796A debris systems would likely have dissipated through radiation pressure "blowout" or infall due to Pointing-Robertson drag (and certainly so for α Psc A), if not replenished (by collisional erosion of planetesimals) and/or dynamical confinement by resonances with yet undetected planetary-mass bodies. The HD 32297 disk cannot be placed in a proper evolutionary context until its age is better constrained.

The break in HD 32297's radial SB profile could arise from a change in the surface density of scattering grains or differentiation in their properties with distance from the star. The latter cannot explain the NE/SW SB profile asymmetries. In the cases of HR 4796A and HD 141569A, the presence of their M star companions may explain the outer "truncation" of their disks (e.g., see Clampin et al. 2003). The explanations for more complex asymmetries may rest in disk/planet dynamics. Evidence of planets in previously imaged debris systems, and possibly also in HD 141569A, has been offered given the asymmetries in their disks. Azimuthal asymmetries could be explained by the presence of undetected planets altering an otherwise azimuthally symmetric dust density distribution by gravitational perturbations (e.g., Ozernoy et al. 2000). Such a mechanism might also be responsible for the SB asymmetries in HD 32297's disk. While still represented by a very small sample, the occurrence (and diversity) of azimuthal asymmetries in the circumstellar disks of A stars seems to be the rule rather than the exception.

8. SUMMARY

We have imaged a circumstellar disk about HD 32297 in 1.1 μm light. The disk, inclined $10\overset{\circ}{.}5 \pm 2\overset{\circ}{.}5$ from edge-on with a major-axis P.A. $= 236\overset{\circ}{.}5 \pm 1^\circ$, extends at least $3\overset{''}{.}3$ (400 AU) from the star. We estimate the 1.1 μm disk flux density beyond the $0\overset{''}{.}3$ radius region obscured by the coronagraph to be 4.81 ± 0.57 mJy, leading to a 1.1 μm disk scattering fraction of 0.0033 ± 0.0004. We find evidence of hemispheric radial brightness asymmetries in the disk that might be attributed to an azimuthally anisotropic distribution of the disk grains, possibly due to the influence of planetary dynamics.

We thank our GO 10177 collaborators for their contributions. Support for this work was provided by NASA through GO grant 10177 from STScI, operated by AURA, Inc., under NASA contract NAS5-26555.

REFERENCES

Ardila, D. R., et al. 2004, ApJ, 617, L147
Bushouse, H. 1997, in The 1997 *HST* Calibration Workshop, with a New Generation of Instruments, ed. S. Casertano & C. Skinner (Baltimore: STScI), 223
Clampin, M., et al. 2003, AJ, 126, 385
Cutri, R. M., et al. 2003, 2MASS All-Sky Catalog of Point Sources (Pasadena: Caltech)
Decin, G., Dominik, C., Waters, L. B. F. M., & Waelkens, C. 2003, ApJ, 598, 636
Jura, M., Malkan, M., White, R., Telesco, C., Pina, & Fisher, R. S. 1998, ApJ, 505, 897
Kalas, P., Graham, J. R., & Clampin, M. 2005, Nature, 435, 1067
Kalas, P., & Jewitt, D. 1995, AJ, 110, 794
Kalas, P., Larwood, J., Smith, B. A., & Schultz, A. 2000, ApJ, 530, L133
Krist, J. E., et al. 2005, AJ, 129, 1008
Larwood, J. D., & Kalas, P. G. 2001, MNRAS, 323, 402
Noll, K., et al. 2004, NICMOS Instrument Handbook, Ver. 7.0 (STScI: Baltimore)
Ozernoy, L. M., Gorkavyi, N. N., Mather, J. C., & Taidakova, T. A. 2000, ApJ, 537, L147
Perryman, M. A. C., et al. 1997, A&A, 323, L49
Schneider, G. 2002, in The 2002 *HST* Calibration Workshop, ed. S. Arribas, A. Koekemoer, & B. Whitmore (Baltimore: STScI), 250 (SCH02)
Schneider, G., Becklin, E. E., Smith, B. A., Weinberger, A. J., Silverstone, M., & Hines, D. C. 2001, AJ, 121, 525 (SCH01)
Schneider, G., & Stobie, E. 2002, in ASP Conf. Ser. 281, Astronomical Data Analysis Software and Systems XI, ed. D. A. Bohlender, D. Durand, & T. H. Handley (San Francisco: ASP), 382
Schneider, G., Wood, K., Silverstone, M. D., Hines, D. C., Koerner, D. W., Whitney, B. A., Bjorkman, J. E., & Lowrance, P. J. 2003, AJ, 125, 1467
Schneider, G., et al. 1999, ApJ, 513, L127
Stobie, E., Lytle, D., Barg, I., & Ferro, A. 1998, in NICMOS and the VLT: A New Era of High Resolution Near Infrared Imaging and Spectroscopy, ed. W. Freudling & R. N. Hook (Garching: ESO), 76
Weinberger, A. J., Becklin, E. E., Schneider, G., Smith, B. A., Lowrance, P. J., Silverstone, M. D., Zuckerman, B., & Terrile, R. J. 1999, ApJ, 525, L53